Journal of Physics: Condensed Matter

Simultaneous antiferromagnetic Fe^{3+} and Nd^{3+} ordering in $NdFe_3(^{11}BO_3)_4$

To cite this article: P Fischer *et al* 2006 *J. Phys.: Condens. Matter* **18** 7975

INSTITUTE OF PHYSICS PUBLISHING JOURNAL OF PHYSICS: CONDENSED MATTER

J. Phys.: Condens. Matter **18** (2006) 7975–7989 doi:10.1088/0953-8984/18/34/010

Simultaneous antiferromagnetic Fe^{3+} and Nd^{3+} ordering in $NdFe_3(^{11}BO_3)_4$

P Fischer[1,4], V Pomjakushin[1], D Sheptyakov[1], L Keller[1], M Janoschek[1,2], B Roessli[1], J Schefer[1], G Petrakovskii[3], L Bezmaternikh[3], V Temerov[3] and D Velikanov[3]

[1] Laboratory for Neutron Scattering, ETH Zürich & Paul Scherrer Institut, CH-5232 Villigen PSI, Switzerland
[2] Physik Department E21, TU München, D-85748 Garching, Germany
[3] Institute of Physics SB RAS, Krasnoyarsk 660036, Russia

E-mail: Peter.Fischer@psi.ch

Received 30 May 2006, in final form 16 July 2006
Published 7 August 2006
Online at stacks.iop.org/JPhysCM/18/7975

Abstract

By means of magnetic susceptibility and specific heat measurements, x-ray and unpolarized neutron diffraction investigations on powder and single-crystal samples, simultaneous long-range antiferromagnetic Fe and Nd ordering in $NdFe_3(^{11}BO_3)_4$ with $R32$ chemical structure has been found at temperatures below $T_N = 30.5(5)$ K down to 1.6 K. At temperatures down to 19 K the propagation vector is $\mathbf{k}_{hex} = [0, 0, 3/2]$ and becomes slightly incommensurate at lower temperatures. Combined with symmetry analysis, best powder neutron profile fits are obtained with magnetic spiral configurations with the magnetic moments oriented parallel to the hexagonal basal plane according to the irreducible representations τ_3 in the commensurate case. This is in agreement with the easy directions of magnetization perpendicular to the c-axis as determined by magnetic susceptibility measurements. At 1.6 K the magnetic Fe moment amounts to 4.9 μ_B close to the free ion moment of Fe^{3+}. The magnetic Nd^{3+} moment saturates presumably due to crystal-field effects at 2.7 μ_B.

1. Introduction

As promising materials for optoelectronics, cf. e.g. [1, 2], and with respect to interesting magnetic properties due to competing magnetic sublattices and magnetoelectric interactions [3–7], the family of borates $RM_3(BO_3)_4$ with R = rare earths or Y, La–Lu and M = Al, Ga, Cr, Fe, Sc is of current interest. Concerning technical applications such compounds,

[4] Author to whom any correspondence should be addressed.

Table 1. Structural parameters of $NdFe_3(^{11}BO_3)_4$, refined from the HRPT neutron diffraction data ($\lambda = 1.8857(5)$ Å) at room temperature, compared to laboratory and synchrotron x-rays (first and second lines of x-ray lattice parameters) as well as to the single-crystal x-ray results of [1]. Space group $R32$ (no 155). B = isotropic temperature factor. Within brackets estimated standard deviations are given, referring to the last relevant digit. Agreement values [15] concerning weighted profile intensities $R_{wp} = 6.8\%$, statistically expected value $R_{exp} = 2.2\%$, goodness of fit $\chi^2 = 10.3$ and concerning integrated nuclear neutron intensities $R_{Bn} = 7.5\%$.

Lattice parameters (Å):	$a_{hex,n} = 9.589(1)$,	$c_{hex,n} = 7.612(1)$,
	$a_{hex,x} = 9.5878(3)$,	$c_{hex,x} = 7.6103(3)$,
	9.588(1),	7.611(1),
	9.578(1),	7.605(3) [1].

Atom	Site	x	y	z	B (Å^2)
Nd	3a	0	0	0	0.38(7)
Fe	9d	0.5500(2)	0	0	0.1[a]
[1]		0.5511(1)			
B1	3b	0	0	0.5	0.47(4)
B2	9e	0.4463(3)	0	0.5	0.47(4)
		0.446(1)			
O1	9e	0.8539(4)	0	0.5	0.66(3)
		0.8557(6)			
O2	9e	0.5948(3)	0	0.5	0.66(3)
		0.5903(8)			
O3	18f	0.4546(2)	0.1448(2)	0.5174(3)	0.66(3)
		0.4511(6)	0.1453(6)	0.5188(6)	

[a] Fixed, as it tended to negative values.

e.g. $YAl_3(BO_3)_4$, may be important materials for laser techniques and optical second harmonic generation [8]. $GdFe_3(BO_3)_4$ has been found [6, 7] to exhibit a structural phase transition at 156 K, antiferromagnetic order of the magnetic Fe^{3+} moments at 36 K, followed by a spin reorientation phase transition at 9 K. Moreover, there is evidence for an induced ferroelectric phase in this material in external magnetic fields which demonstrates a strong correlation between the magnetic order and the dielectric properties of $GdFe_3(BO_3)_4$. The understanding of the physical properties of such multiferroic materials with coexistence of magnetic and ferroelectric ordering is currently of topical interest, see e.g. [9, 10].

By means of single-crystal x-ray diffraction measurements, the chemical structures of the borates $RM_3(BO_3)_4$ have been determined to belong to the huntite ($CaMg_3(CO_3)_4$) type chemical structure according to the noncentrosymmetric trigonal space group $R32$ (no 155) [1, 6]. Rare-earth iron borates of heavy rare earths and of Y undergo also a structural phase transition at higher temperatures with symmetry change to space group $P3_121$ (no 152) [7].

At room temperature the compound $NdFe_3(BO_3)_4$ has the lattice parameters $a_{hex} = 9.578$ Å and $c_{hex} = 7.605$ Å [1] in the hexagonal setting. The magnetic Nd and Fe atoms occupy the special sites (3a), 0, 0, 0, and (9d), $x, 0, 0$, with $x = 0.5511(1)$ [1], respectively. Further structural parameters are summarized in table 1.

Using a SQUID, DC magnetic measurements were performed by Campà *et al* on $NdFe_3(BO_3)_4$ in an external magnetic field of 1 kOe at temperatures down to 1.8 K [1]. Two peaks in magnetic susceptibility were observed at approximately 33(2) K and at 6 K. The authors assumed magnetic order within the Fe sublattice at the higher temperatures and three-dimensional antiferromagnetic ordering of both the Fe^{3+} and Nd^{3+} sublattices at temperatures below 6 K. By means of infrared absorption spectroscopy later Chukalina *et al* [2] confirmed the Néel temperature $T_N = 33(1)$ K and proposed simultaneous magnetic ordering of the two

magnetic sublattices. Moreover, at 4.2 K a ground state exchange splitting of approximately 1.1 meV has been deduced from these measurements.

With respect to these different models of magnetic sublattice interactions and in view of the strong neutron absorption by Gd, we decided to determine the magnetic ordering of $NdFe_3(BO_3)_4$ as a prototype of $RFe_3(BO_3)_4$ by means of bulk magnetic and unpolarized neutron diffraction investigations on powder and single-crystal samples, in combination with group-theoretical symmetry analysis. To our knowledge, such results have not been previously reported for the interesting class of $RFe_3(BO_3)_4$ borates of rare earths R.

2. Sample preparation

Because of the strong neutron absorption by natural boron, samples with ^{11}B enriched to 99% were prepared at the Institute of Physics at Krasnoyarsk. The single crystals $NdFe_3(^{11}BO_3)_4$ were grown from solution in a melt [11] of 75 mass% $(Bi_2Mo_3O_{12} + 3\ ^{11}B_2O_3 + 0.6Nd_2O_3) + 25$ mass% $NdFe_3(^{11}BO_3)_4$. The saturation temperature was $T_s \approx 920\,^{\circ}C$, and the concentration (n) dependence of T_s was $dT_s/dn = 5\,^{\circ}C/\text{mass\%}$. The flux with mass of 150 g was prepared by melting at the temperature of 1100 °C of the oxides Bi_2O_3, MoO_3, $^{11}B_2O_3$, Fe_2O_3 and Nd_2O_3, using a platinum crucible. The flux was kept at this temperature for 10 h for homogenization. Afterwards the temperature of the flux was decreased to $T = T_s + 7\,^{\circ}C$, the platinum rod with four seeds was settled down in the flux and the rotation of 30 revolutions per minute of the rod was switched on. After 10 min the temperature was decreased to $T = T_s - 10\,^{\circ}C$. Then the temperature was decreased with velocity of 1–3 °C/24 h. The total duration of the crystal growth was about 14 days. Thus crystals with linear dimensions up to 12 mm were prepared.

3. Experimental details

Magnetic susceptibility measurements were made by means of a SQUID at the Institute of Physics at Krasnoyarsk on a single crystal of $NdFe_3(BO_3)_4$ in the temperature range from 4.2 to 224 K. In addition the temperature dependence of specific heat of polycrystalline $NdFe_3(^{11}BO_3)_4$ was determined using PPMS from Quantum Design at Paul Scherrer Institut in the temperature range from approximately 3 to 152 K. From about 15 to 43 K a measurement in an external magnetic field of 9 T has also been performed.

A small part of the $NdFe_3(^{11}BO_3)_4$ powder sample has been examined on the Siemens D-500 laboratory x-ray powder diffractometer of the Paul Scherrer Institut at room temperature in the $\theta/2\theta$ geometry (flat sample, rotating) with Cu Kα radiation.

In addition, some of the $NdFe_3(^{11}BO_3)_4$ powder was filled into a cylindrical glass capillary of approximately 0.3 mm diameter and 0.9 mm length and was measured at 308 K on the high resolution powder diffractometer at the Swiss SLS synchrotron of Paul Scherrer Institut. X-rays of wavelength $\lambda = 0.708\,27(5)$ Å and a microstrip detector were used. The sample had been rotating during the measurement. The final average diffraction pattern covers the scattering angle range from 3.519° to 70.151° with an angular step of 0.004°.

For powder neutron diffraction measurements single crystals of $NdFe_3(^{11}BO_3)_4$ were crushed to a fine powder and a cylindrical V container of 8 mm diameter and 55 mm height filled under He gas atmosphere. For the neutron wavelength of 1.8857(5) Å the sample transmission has been measured, yielding the product of linear absorption coefficient μ and sample radius r: $\mu r = 0.344$. For cooling, ILL type cryostats were used.

At room temperature a powder neutron diffraction measurement was made at the high-resolution powder neutron diffractometer HRPT [12] at the continuous spallation neutron

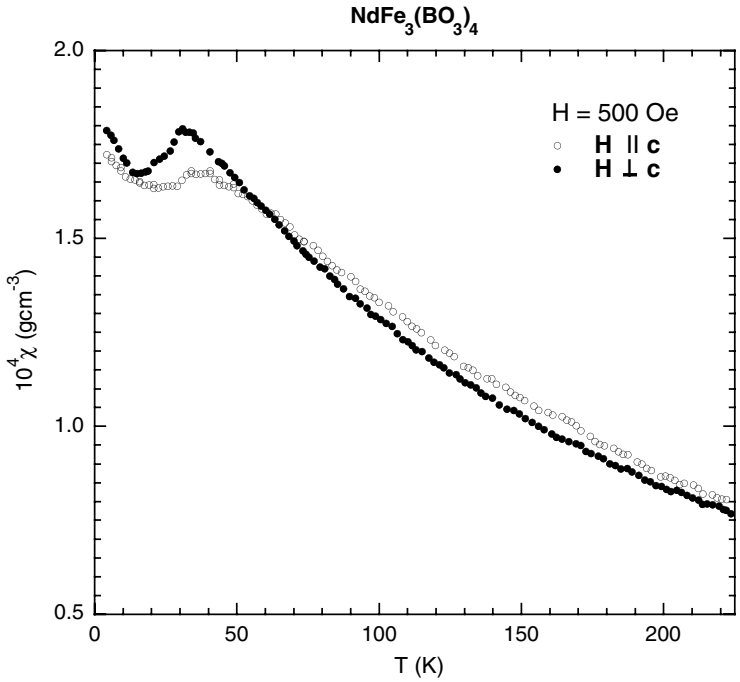

Figure 1. Anisotropy of magnetic susceptibility, measured by means of a SQUID at the Institute of Physics at Krasnoyarsk on a $NdFe_3(BO_3)_4$ single crystal with magnetic field H applied parallel and perpendicular to the hexagonal c-direction.

source SINQ of Paul Scherrer Institut. The neutron wavelength $\lambda = 1.8857(5)$ Å, the high intensity mode of the instrument without primary Soller collimator and rotation of the sample has been used. Low-temperature measurements were first made with a stationary sample on the cold-neutron powder diffractometer DMC [13] at SINQ with neutron wavelength $\lambda = 2.4526(5)$ Å at temperatures down to 1.6 K. Subsequent DMC measurements were made with an oscillating sample in order to reduce preferred orientation effects or rather to obtain a better powder averaging over crystallite grains. This procedure improved the fits considerably. It should be mentioned that due to the Ge monochromator of HRPT and the pyrolytic graphite filter used at DMC, higher order contaminations of the neutron beam were negligible.

Further investigations were performed on a $NdFe_3(^{11}BO_3)_4$ single crystal of approximate dimensions $8 \times 8 \times 8$ mm^3 by means of the thermal neutron diffractometer TriCS [14] at SINQ in the single-detector mode of operation at temperatures down to approximately 5 K, using the neutron wavelength $\lambda = 1.1809(4)$ Å.

The diffraction data were analysed with recent versions of the FullProf program system [15] with the internal neutron scattering lengths (assuming ^{11}B) and neutron magnetic form factors.

4. Results of bulk magnetic measurements

Figure 1 clearly illustrates that at low temperatures the easy directions of magnetization are in the case of $NdFe_3(BO_3)_4$ oriented perpendicular to the hexagonal c-axis. The corresponding peak of magnetic susceptibility at approximately 31(1) K suggests the onset of antiferromagnetic ordering. Below approximately 15 K there is again an increase of this

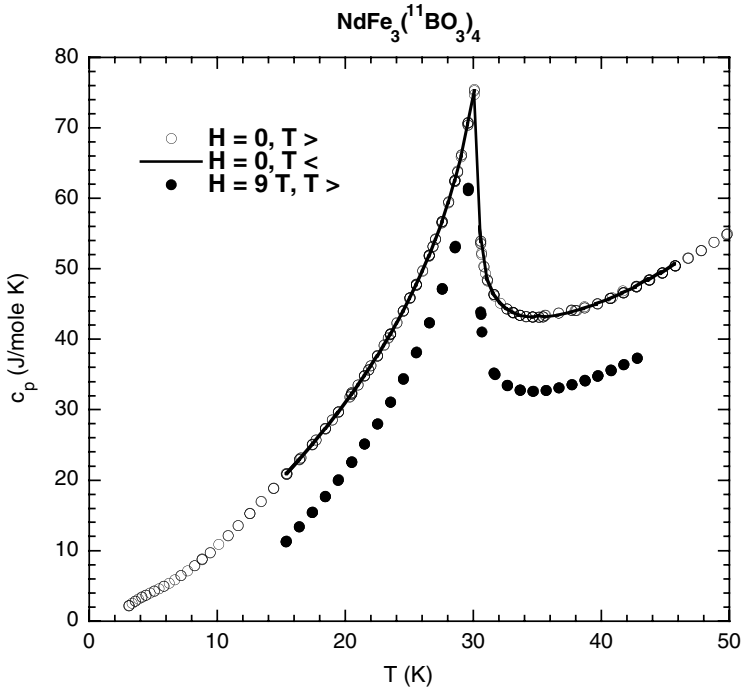

Figure 2. Temperature dependence of the specific heat of polycrystalline $NdFe_3(^{11}BO_3)_4$, measured on the PPMS (Quantum Design) at Paul Scherrer Institut. For clarity the data points in an external magnetic field of 9 T have been shifted by −10 units. $T >$ and $<$ indicate increasing and decreasing temperature, respectively.

magnetic susceptibility for lower temperatures. On the other hand, the peak at 6 K, reported in [1], is not seen.

Also the specific heat measurements performed on $NdFe_3(^{11}BO_3)_4$, which are illustrated in figure 2, only exhibit a single peak at approximately 30.1(2) K due to the onset of long-range magnetic order, without significant hysteresis in zero external magnetic field as well as with almost no shift of this peak in an external magnetic field of 9 T.

5. Powder x-ray and neutron diffraction refinements of the chemical structure

In the powder profile matching mode [15], the laboratory x-ray diffraction pattern measured on a polycrystalline $NdFe_3(^{11}BO_3)_4$ specimen at room temperature can be excellently fitted (goodness of fit $\chi^2 = 3.5$, $R_{Bn} = 2.6\%$ concerning integrated nuclear neutron intensities [15]) on the basis of space group $R32$, yielding the lattice parameters listed in table 1. However, there is additional intensity close to the first Bragg peak (1, 0, 1) which is visible as a shoulder towards higher scattering angles. It may be due to a trace of $Nd(OH)_3$. Otherwise the sample seems to be the expected single-phase borate material. On the other hand, fits with the structure model published in [1] reveal very strong preferred orientation along the direction [1, 0, 1] and produce only moderate agreement between observation and calculation.

In contrast to the expectations, the synchrotron x-ray test measurement yielded at 308 K no evidence for the presence of other phases or additional line splittings. The observed Bragg peaks may be well indexed on the basis of space group $R32$ with the hexagonal lattice parameters given in table 1.

As neutrons are in contrast to x-rays particularly sensitive to light atoms such as boron and oxygen, a powder profile refinement of the HRPT data for room temperature was also made starting from the structure model published in [1]. Corresponding refined structural parameters are summarized in table 1. Despite sample rotation, the powder intensities still indicate certain problems associated with preferred orientation or insufficient powder averaging. Normally the former effect is small in the case of neutron diffraction. Using the March approach for preferred orientation [15], the fits improved essentially, but in contrast to x-rays no well defined preferred orientation direction was found and finally has been fixed to the direction [0, 0, 1]. 101 reflections contribute to the neutron diffraction pattern, compared to 27 parameters used in the refinement (six for the background polynomial). Within error limits, the lattice parameters of the present $NdFe_3(^{11}BO_3)_4$ sample determined by x-ray and neutron diffraction agree, but are somewhat larger than the values published in [1] for $NdFe_3(BO_3)_4$. The positional parameters are in reasonable agreement with those published by Campá *et al* [1].

6. Magnetic ordering of the Nd and Fe sublattices

6.1. Determination of the propagation vectors $\boldsymbol{k}_j$

The low-temperature neutron diffraction patterns measured on the DMC diffractometer contain additional magnetic Bragg peaks, which prove long-range magnetic ordering in $NdFe_3(^{11}BO_3)_4$. By means of powder profile matching [15], these peaks may be well indexed by means of propagation vector $\mathbf{k}_{\rm hex} = [0, 0, 3/2]$. Within the resolution of the 2.453 Å powder neutron diffraction measurements, this holds for the entire low-temperature range.

Single-crystal investigations on $NdFe_3(^{11}BO_3)_4$, performed on the neutron diffractometer TriCS, confirm that at temperatures $\geqslant$ 19 K $\mathbf{k}_{\rm hex} = [0, 0, 3/2]$. The observed magnetic peaks such as $(-1, 0, 1/2) = (-1, 0, -1 + 3/2)$ appear as satellites $\pm\mathbf{k}$ of nuclear Bragg peaks which fulfil the R lattice condition $-h + k + l = 3n$, $n =$ integer.

However, in contrast to the magnetic reflection $(0, 0, 3/2)$ appearing at temperatures below 33 K, a slight incommensurability corresponding to $\mathbf{k}^i_{\rm hex} = [0, 0, 3x = 3/2 + \varepsilon]$ has been detected by the observed splitting of the magnetic peak $(-1, 0, 1/2)$ at temperatures below approximately 19 K which is illustrated in figure 3. In the q-scan along L (see figure 3(b)) the deviation ΔL from $1/2$ is rather small: of the order of 0.005. Therefore we currently also cannot exclude for $NdFe_3(^{11}BO_3)_4$ within the resolution of TriCS at the used neutron wavelength of 1.181 Å the presence of a $\mathbf{k}$-vector component perpendicular to the z-direction. Further similar studies with cold neutrons will be necessary to distinguish between the latter two cases.

6.2. Symmetry analysis

Based on the determined propagation vectors $\mathbf{k}_j$, we performed a symmetry analysis according to Izyumov and Naish [16] to derive possible magnetic structures for the Fe and Nd sublattices, considering the magnetic moments as axial vectors in a Fourier expansion containing the $\mathbf{k}_j$ vectors and the irreducible representations of the space group of the chemical structure. For this purpose we used programs MODY [17] and BASIREP [15] to obtain the corresponding, magnetic modes (basis vectors $\boldsymbol{\Psi}_j(0)$ in Fourier space). By means of suitable linear combinations [17] formed from these in general complex functions for $\pm\mathbf{k}$, one obtains the required magnetic configurations for the zeroth chemical unit cell in real space. Moreover, one may relate according to Izyumov and Naish [16] $\boldsymbol{\Psi}_j(\mathbf{t})$ of the chemical unit cell displaced by translation $\mathbf{t}$ to $\boldsymbol{\Psi}_j(0)$ by means of the equation

$$\boldsymbol{\Psi}_j(\mathbf{t}) = \boldsymbol{\Psi}_j \exp(\mathrm{i}2\pi\mathbf{kt}), \tag{1}$$

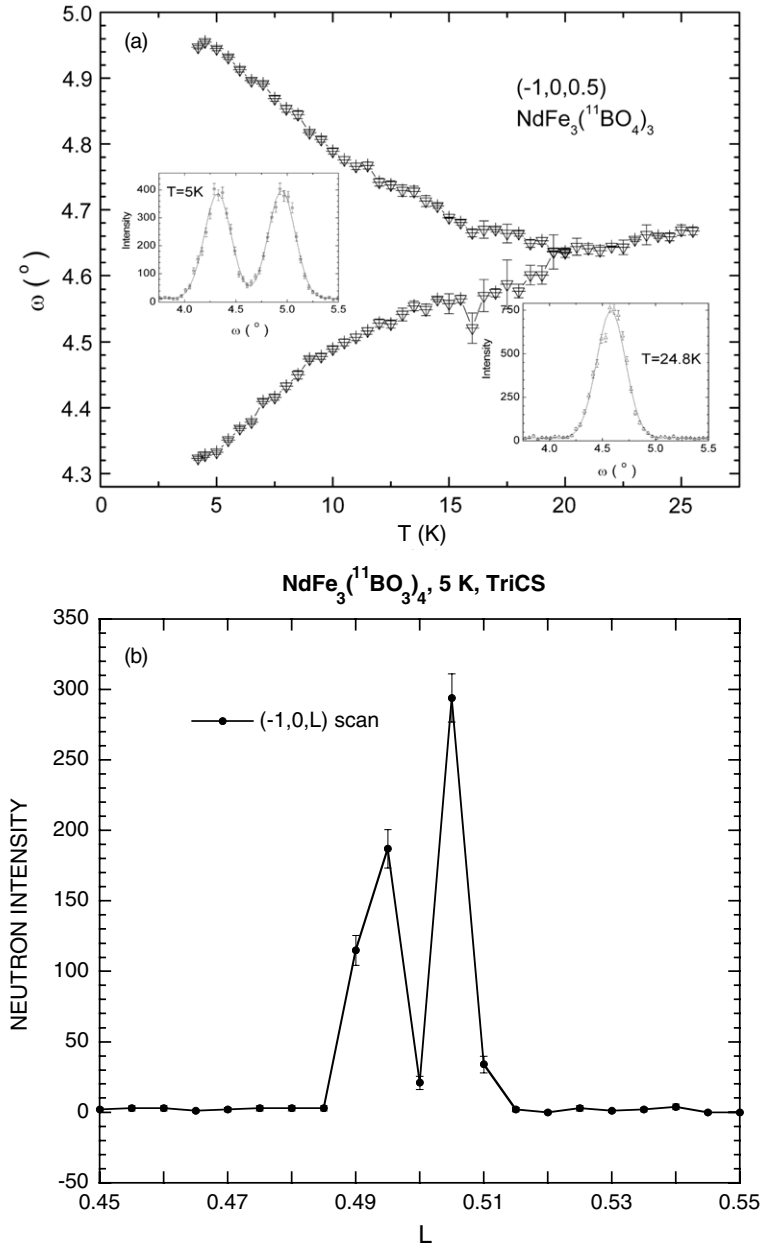

Figure 3. (a) ω scan (turning around the b-axis) of the $(-1, 0, 1/2)$ magnetic peak of $NdFe_3(^{11}BO_3)_4$ as a function of temperature. (b) $(-1, 0, L)$-scan of $NdFe_3(^{11}BO_3)_4$ centred at $L = 1/2$ for the temperature of 5 K, yielding two incommensurate magnetic peaks such as $(-1, 0, -1 + 1.505)$ and $(-1, 0, 2 - 1.505)$.

where **t** is a translation vector from the zeroth cell to the νth cell or is a rhombohedral centring translation in the hexagonal description. It has been pointed out by the previously mentioned authors that one has to use the primitive, i.e. the rhombohedral, unit cell with respect to the translations. This implies in the hexagonal description that the atoms related

by the rhombohedral R translations $(+(0, 0, 0; 2/3, 1/3, 1/3; 1/3, 2/3, 2/3))$ are no longer equivalent as is the case for such chemical structures, but differ by phase factors $2\pi\mathbf{kt}$ according to these translations. Keeping this in mind, we discuss in the following only the symmetry relations for the first of these three R sublattices in the hexagonal frame.

For the incommensurate case with propagation vector $\mathbf{k} = \mathbf{k}^i_{\rm hex} = [0, 0, 3x = 3/2 + \varepsilon]$, there exist three irreducible representations τ_1, τ_2 and τ_3. All three are one dimensional: the first one is real, and the other two are conjugate complex. They are summarized in appendix A together with the magnetic modes for the irreducible representation τ_2, which yielded the best fit of the measured magnetic neutron intensities.

In the commensurate case with propagation vector $\mathbf{k} = \mathbf{k}_{\rm hex} = [0, 0, 3/2]$ there are also three irreducible representations τ_1, τ_2 and τ_3. The first two are one dimensional and real, whereas the third one is two dimensional (in this case one has to form linear combinations of Ψ_{jm}). They are summarized in appendix B together with the magnetic modes for the irreducible representation τ_3, which yielded the best fit of the measured magnetic neutron intensities.

As we know from magnetic susceptibility that the easy directions of magnetization are perpendicular to the hexagonal c-axis, we search for magnetic configurations in the hexagonal basal plane, i.e. we use only the Ψ_1 and Ψ_2 basis vectors for the magnetic Fe moment for the incommensurate $\mathbf{k}$. For the Nd site the magnetic moment is restricted to be in the basal plane. Since the $-\mathbf{k}$ propagation vector is not equivalent to the $+\mathbf{k}$ one, one has to find proper mixing coefficients using both sets of basis vectors $\Psi(+\mathbf{k})$ and $\Psi(-\mathbf{k})$, which are listed in appendix A. However, in the present case we can always make the basis vectors of $-\mathbf{k}$ complex conjugated to ones of $+\mathbf{k}$ by using the following linear combinations for both Fe and Nd sites:

$$\begin{aligned}\Psi'_1(-\mathbf{k}) &= -a\Psi_1(-\mathbf{k}),\\ \Psi'_2(-\mathbf{k}) &= a(\Psi_1(-\mathbf{k}) + \Psi_2(-\mathbf{k})),\end{aligned} \tag{2a}$$

where $a = \exp(\mathrm{i}\pi/3)$. Thus, the general solution for the magnetic configuration of Fe magnetic moments parallel to the basal plane corresponding to the irreducible representation τ_2 reads

$$\mathbf{S}^{\rm Fe} = \mathrm{Re}[(C_1\Psi^{\rm Fe}_1(+\mathbf{k}) + C_2\Psi^{\rm Fe}_2(+\mathbf{k}))\exp(\mathrm{i}2\pi\mathbf{kt})], \tag{2b}$$

where C_1 and C_2 are arbitrary complex numbers; the basis vectors Ψ_1, Ψ_2 for all three Fe atoms are listed in appendix A.

For the Nd site, the magnetic moment configuration is

$$\mathbf{S}^{\rm Nd} = \mathrm{Re}[C_3\Psi^{\rm Nd}_1(+\mathbf{k})\exp(\mathrm{i}2\pi\mathbf{kt})]. \tag{2c}$$

It is easy to see that the Nd moments form a spiral with constant moment amplitude. The coefficient between the components along x and y of the hexagonal basic vectors amounts to $a = \exp(\mathrm{i}\pi/3)$, providing the necessary phase shift of $\pi/3$. The components along x and y are proportional to $\cos(2\pi kz)$ and $\cos(2\pi kz + \pi/3)$, which set the circular spiral with an arbitrary direction of the magnetic moment inside the basal plane for the zeroth cell.

The Fe moments have in general an elliptical spiral configuration propagating along the z-direction. However, since the propagation vector is almost commensurate ($\mathbf{k} = [0, 0, 3/2]$), the magnetic moments of the atoms generated from those in the basal plane by the rhombohedral lattice centring translations in the nearest neighbouring planes above and below are practically antiparallel, with roughly equal sizes. In the zeroth cell all three Fe moments are in general different and have their mutual orientation according to the mixing coefficients in the equation (2*b*). One important special case of parallel orientation of all three moments in the basal plane is given by choosing $C_2 = C_1a^*$. This linear combination gives the same basis vector for all three atoms in the basal plane proportional to $(1, a^*)$, which corresponds to a spiral configuration with the constant moment size similar to the Nd case. The above

mentioned linear combination is the only one which yields the constant moment configuration. The direction within the plane is not fixed.

It is interesting to note one additional special triangular configuration for $C_2 = 0$ when the Fe moments form a $2\pi/3$ angle with respect to each other:

$$\begin{aligned} \mathbf{S}_1^{\mathrm{Fe}}(\mathbf{t}) &= S\mathbf{e}_x \cos(2\pi\mathbf{kt} + \alpha), \\ \mathbf{S}_2^{\mathrm{Fe}}(\mathbf{t}) &= -S\mathbf{e}_y \cos(2\pi\mathbf{kt} + \pi/3 + \alpha), \\ \mathbf{S}_3^{\mathrm{Fe}}(\mathbf{t}) &= S(\mathbf{e}_x + \mathbf{e}_y) \cos(2\pi\mathbf{kt} - \pi/3 + \alpha), \end{aligned} \tag{3}$$

where $\mathbf{e}_x$ and $\mathbf{e}_y$ are unit vectors along the basic translations of the hexagonal lattice. Equations (3) describe a modulated triangular configuration, but with in the case of zero $\mathbf{t}$ and $\alpha^{\mathrm{Fe}} = 0$ unequal magnitudes (absolute values) of the three magnetic Fe moments: S, $S/2$, $S/2$. As both the Fe and Nd magnetic moments of $NdFe_3(^{11}BO_3)_4$ are more likely to be well localized, spiral type configurations, i.e. with constant magnetic-moment magnitudes, are more probable.

For convenience we give the equation which describes the spiral configuration in the orthogonal basis (and holds for all three magnetic Fe moments as well as similarly for the magnetic Nd moment):

$$\mathbf{S}^{\mathrm{Fe}}(\mathbf{t}) = S^{\mathrm{Fe}}[(\sqrt{3}\mathbf{e}_x \cos(2\pi\mathbf{kt} + \alpha^{\mathrm{Fe}}) + (\mathbf{e}_x + 2\mathbf{e}_y) \sin(2\pi\mathbf{kt} + \alpha^{\mathrm{Fe}})]/\sqrt{3}, \tag{4}$$

where $\mathbf{e}_x$ and $\mathbf{e}_y$ are unit vectors along the basic translations of the hexagonal lattice ($\mathbf{e}_x + 2\mathbf{e}_y$ is perpendicular to $\mathbf{e}_x$), and α is a rotation angle around the z-axis.

For unpolarized neutrons and powder samples or multidomain single crystals with statistical domain distribution, it is only possible to determine the moment magnitudes and relative phase of the Fe and Nd sublattices in the hexagonal basal plane. Therefore we fix α^{Fe} to zero, and refine only α^{Nd} which may be considered as a polar angle ϕ^{Nd} relative to the hexagonal x-axis. Finally we should mention that the above equations hold both for the discussed commensurate and incommensurate magnetic ordering.

6.3. Determination of the magnetic ordering and its temperature dependence

We tried to fit systematically both possible modulated and spiral type magnetic structures to the measured magnetic neutron intensities, but only in the latter case was a good fit obtained. To fit the magnetic contribution of the neutron data at 2 K (difference I(2 K)–I(50 K)) with the general approach, we therefore used equation (2*b*) for the Fe sublattice and equation (2*c*) for the magnetic Nd moment. The imaginary phase of C_1 was fixed to zero. One of the fit parameters of equation (2*b*) should be fixed because one cannot determine the phase shift of the modulated magnetic structure with respect to the crystal lattice from the present experiment with unpolarized neutrons. The fit with five free parameters $\mathrm{Re}(C_1)$, $\mathrm{Re}(C_2)$, $\mathrm{Im}(C_2)$, $\mathrm{Re}(C_3)$ and $\mathrm{Im}(C_3)$ gave the ratio $C_2/C_1 = 1.02\exp(-\mathrm{i}0.44\pi)$ (with error bars 0.05 and 0.02 for the modulus and the phase, respectively), which is quite close to the value of $\exp(-\mathrm{i}\pi/3)$ expected for the parallel Fe moments. The angles between the Fe moments amount to $\sim 10°$, while the sizes of the magnetic moments are 1, 0.9 and 1.2 for the three Fe sites, normalized to the magnetic moment of the first atom. The refined Nd-moment direction with respect to the Fe moments in the hexagonal basal plane is 83°, 64° and 70° for the three Fe moments. The resulting goodness of fit [15] is $\chi^2 = 15.4$. However, we think that the assumption of the equal Fe moments is physically more reasonable and do not contradict the measured powder neutron diffraction data. By fixing $C_2 = C_1\exp(-\mathrm{i}\pi/3)$, we get the only slightly worse goodness of fit $\chi^2 = 16.8$. In this constant magnetic moment case there are only three adjustable parameters, two values of the ordered magnetic moments and an angle between them.

Table 2. Experimental details, resulting ordered magnetic moments μ and agreement values of the neutron powder profile fits of $NdFe_3(^{11}BO_3)_4$ as a function of temperature, measured on DMC, based on the commensurate magnetic unit cell. The polar ϕ angle of the Fe sublattice has been fixed to zero. At 15 K the lattice parameters have been determined as $a_{hex} = 9.594(1)$ Å and $c_{hex} = 7.603(1)$ Å. Note the essential improvements of the nuclear fits due to sample oscillation. With respect to equation (4) $S = \mu$. R_{Bn} and R_{Bm} are conventional R-factors concerning integrated nuclear and magnetic neutron intensities, respectively [15].

T (K)	Sample motion	μ^{Fe} (μ_B)	μ^{Nd}	ϕ^{Nd} (deg)	χ^2	R_{Bn}	R_{Bm}
50	No	0	0		176	15.0	
30	Osc.	1.4(2)	0.5(1.1)	77[b]	77	8.9	47.9
25	Osc.	3.27(8)	1.1(5)	77(3)	61	8.1	11.5
20	Osc.	3.93(7)	1.2(4)	75(3)	57	7.9	7.8
15	Osc.	4.34(6)	1.3(4)	69(4)	55	7.8	6.3
10	No	4.81(4)	2.3(2)	58(1)	20		9.8
1.6	No	4.89(3)[c]	2.7(1)	47(1)	13		8.0
[a]		4.89(4)	2.7(2)	46(2)	18		10.7

[a] $k_{hex} = [0, 0, k_z]$, refined to $k_z = 1.5058(1)$ at 1.6 K.
[b] Fixed value.
[c] Note the expected value $\mu^{Fe} = 5\ \mu_B$ for free Fe^{3+} ions.

For the profile analyses of the DMC powder neutron intensities of $NdFe_3(^{11}BO_3)_4$ with the FullProf program system [15] we finally used equation (4), which resulted in good fits of the magnetic neutron intensities, limited by the previously mentioned texture problems (in particular of the strongest nuclear Bragg peak). In view of the rather limited q-range of the DMC patterns at the long neutron wavelength $\lambda = 2.453$ Å, we fixed the positional parameters to the values summarized in table 1 with an overall temperature factor $B = 0$ and used only 10 or 14 parameters (three for the background polynomial) for nuclear and nuclear + magnetic refinements, respectively. Best agreements were obtained by using separate preferred orientation parameters for the nuclear and magnetic intensities. As these corrections are smaller in the case of magnetic intensities, the discussed problems of the nuclear fits are probably partially associated with deviations in the distributions of the boron and oxygen atoms from the assumed structure model. In the case of a nonoscillating sample we therefore worked with magnetic difference neutron diffraction patterns, visually determined background values and used the lattice parameters determined at 15 K. Typical corresponding fits are illustrated in figure 4. The corresponding commensurate magnetic structure is shown in figure 5.

The temperature dependences of the resulting ordered magnetic Fe and Nd moments of $NdFe_3(^{11}BO_3)_4$ are illustrated in figure 6, and corresponding further details are summarized in table 2.

7. Discussion and conclusions

Bulk magnetic measurements performed on the trigonal rare-earth borate $NdFe_3(BO_3)_4$ with interesting optical properties indicate the onset of antiferromagnetic ordering at temperatures below the Néel temperature of 30.5(5) K and prove easy plane magnetization perpendicular to the hexagonal c-axis.

Although x-ray single-crystal studies determined the chemical structure of $NdFe_3(BO_3)_4$ as belonging to the noncentrosymmetric space group $R32$ [1], the present neutron diffraction results leave some doubt on the correctness of the derived chemical structure, in particular with respect to the distribution of boron and oxygen atoms. Possibly the overall symmetry is only

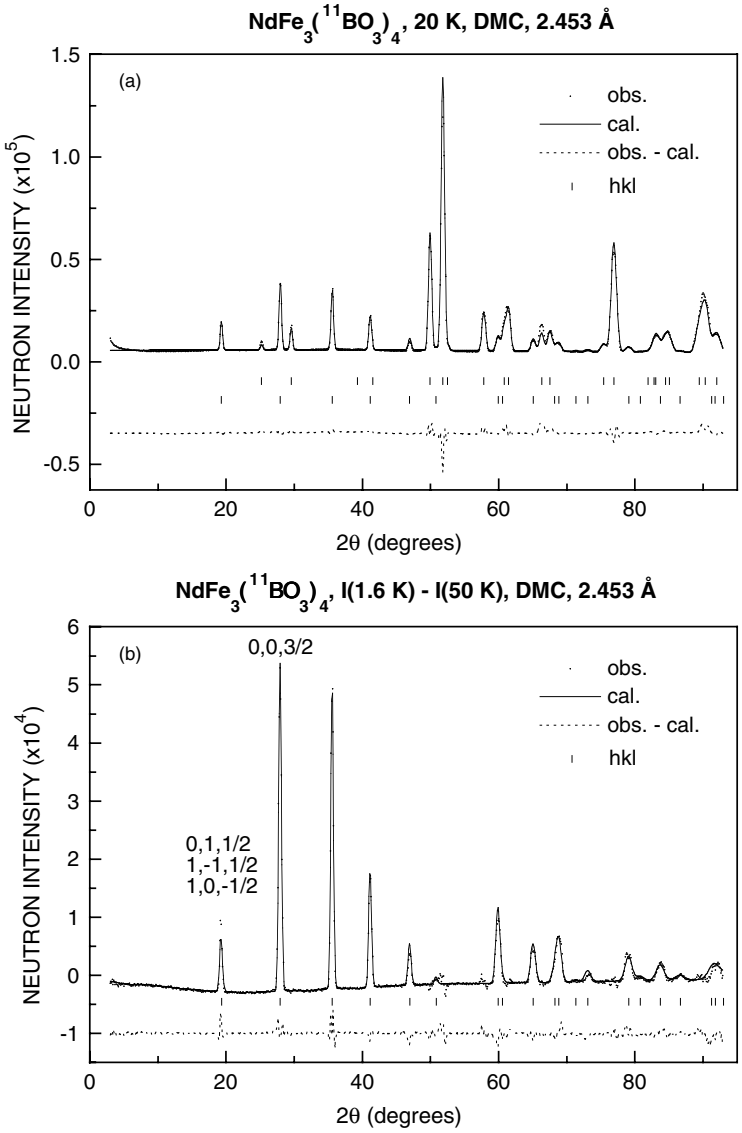

Figure 4. (a) Observed (points, angular step 0.1°), calculated (line) and difference neutron diffraction pattern of $NdFe_3(^{11}BO_3)_4$ at 20 K. The upper and lower vertical bars show nuclear and magnetic Bragg peak positions, respectively. (b) Observed (points, magnetic intensities), calculated (line, for commensurate magnetic unit cell) and difference neutron diffraction pattern of $NdFe_3(^{11}BO_3)_4$ at 1.6 K.

*R*3. On the other hand, particularly the neutron diffraction data with nonoscillating sample were essentially affected by preferred orientation and insufficient powder averaging.

By means of unpolarized neutron diffraction investigations on powder and single-crystal samples of $NdFe_3(^{11}BO_3)_4$, to our knowledge for the first time simultaneous long-range antiferromagnetic iron and rare-earth ordering at low temperatures down to 1.6 K has been established in the interesting class of rare-earth borates $RFe_3(BO_3)_4$ comprising multiferroic materials such as the strongly neutron absorbing compound $GdFe_3(BO_3)_4$ [6]. It corresponds

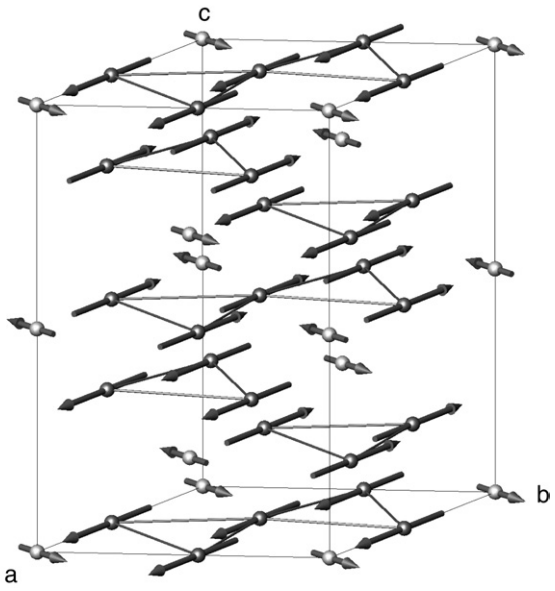

Figure 5. Hexagonal magnetic unit cell of $NdFe_3(^{11}BO_3)_4$ at 20 K, plotted with program ATOMS [18]. Dark grey/grey spheres and arrows illustrate the Fe and Nd atoms and their magnetic moments, respectively.

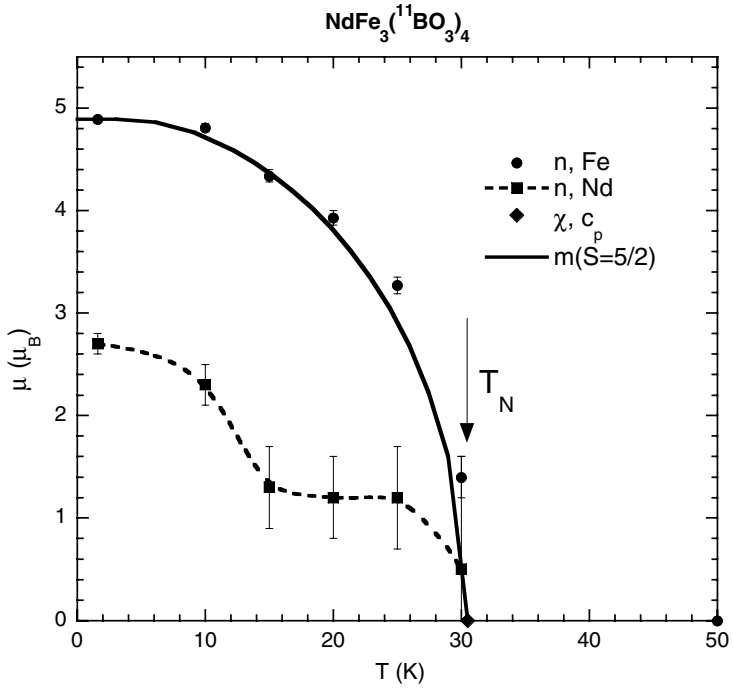

Figure 6. Temperature dependences of the ordered magnetic Fe and Nd moments of $NdFe_3(^{11}BO_3)_4$ with error bars according to estimated standard deviations, see table 2. The full and dashed lines are the expected magnetization (m) curve for $S = 5/2$ [19] and a guide to the eye, respectively.

to the propagation vector $\mathbf{k}_{\rm hex} = [0, 0, 3/2]$ at $T \geqslant 19$ K, which seems to hold also at lower temperatures in the case of powder neutron diffraction. However, based on the single-crystal neutron diffraction results obtained on diffractometer TriCS, there is evidence for a slight

incommensurability according to a propagation vector $\mathbf{k}^i_{\rm hex} = [0, 0, 3x = 3/2 + \varepsilon]$ or perhaps a more general **k**-vector at temperatures below 19 K. To distinguish between the latter two cases, further neutron diffraction studies are needed on $NdFe_3(^{11}BO_3)_4$ single crystals with cold neutrons.

Symmetry analysis combined with neutron powder profile analysis yield best fits for magnetic spiral configurations with the magnetic moments oriented parallel to the hexagonal basal plane according to the irreducible representations τ_3 and τ_2 for the discussed commensurate and incommensurate cases, respectively, in agreement with the easy directions of magnetization observed by magnetic susceptibility measurements. As illustrated in figure 5, the magnetic moments of each sublattice are collinear, and there is antitranslation along the hexagonal *c*-axis. The magnetic neutron diffraction patterns measured on DMC may be well fitted at all temperatures by the commensurate magnetic structure, and possible deviations from it are small (see figure 4(b) and table 2). At 1.6 K the magnetic Fe moment amounts to 4.9 $\mu_{\rm B}$ close to the free ion moment of Fe^{3+}, and Nd^{3+} saturates at 2.7 $\mu_{\rm B}$, presumably due to crystal-field effects. The temperature dependence of the ordered magnetic Fe moment follows approximately the theoretical expectation for the spin value $S = 5/2$; see figure 6. Apart from a possible abrupt increase in the ordered magnetic Nd moment at approximately 15 K (see figure 6), which may be associated with the commensurate–incommensurate phase transition, the observed neutron intensities do not provide evidence for another magnetic phase transition occurring in $NdFe_3(^{11}BO_3)_4$ at lower temperatures. This is in contrast to magnetic susceptibility measurements published in [1] and rather confirms the specific heat results and the optical studies of [2]. On the other hand, there occurs a continuous change in the orientation of the magnetic Nd moments relative to the magnetic Fe moments from 77° at 25 K to 47° at 1.6 K. Presumably this is caused by the increasing internal magnetic field due to the Fe moments which tends to reorient the Nd moments closer to the direction of the Fe moments.

It should be interesting to verify the determined magnetic structures by means of zero-field neutron polarimetry on single crystals and thus—if possible in the case of magnetic domains—also to fix the absolute orientation of the magnetic moments in the hexagonal basal plane.

Acknowledgments

The neutron diffraction investigations were performed at the continuous spallation neutron source SINQ, and the specific heat measurements were made on PPMS (department LDM) from Quantum Design at Paul Scherrer Institut at Villigen PSI in Switzerland. The authors thank them for the provided neutron beam time and Professor B Patterson *et al* from SLS for the test time. Moreover we are indebted to Professor W Sikora, AGH University of Science and Technology, Krakow, for the program MODY and stimulating discussions on the symmetry analysis. This work was financially supported by the Russian Foundation for Basic Research, project no 06-02-16255.

Appendix A

Table A.1. Irreducible representations $\tau_{\rm s}$ and magnetic modes $\mathbf{\Psi}_j$ (with components along the hexagonal basic translations), as obtained from the program MODY [17] for irreducible representation τ_2 and $\mathbf{k} = [0, 0, 3x = 3/2 + \varepsilon]$, $a = \exp(i\pi/3)$, $b = \exp(i\pi/6)$.

Sym. op./Irred. rep.	1	3^+	3^-
τ_1	1	1	1
τ_2	1	$-a^*$	$-a$
τ_3	1	$-a$	$-a^*$

Table A.1. (Continued.)

(a) Fe sublattice (there is only one orbit): representation $\tau = 3\tau_1 + 3\tau_2 + 3\tau_3$			
Atom no (position)	j	$\mathbf{\Psi}_j(\mathbf{k})$	$\mathbf{\Psi}_j(-\mathbf{k})$
1 $(x, 0, 0)$	1	$(1, 0, 0)$	$(-a^*, 0, 0)$
	2	$(0, 1, 0)$	$(a^*, a^*, 0)$
	3	$(0, 0, 1)$	$(0, 0, a^*)$
2 $(0, x, 0)$	1	$(0, -a, 0)$	$(0, -a, 0)$
	2	$(a, a, 0)$	$(-a, 0, 0)$
	3	$(0, 0, -a)$	$(0, 0, a)$
3 $(1 - x, 1 - x, 0)$	1	$(a^*, a^*, 0)$	$(-1, -1, 0)$
	2	$(-a^*, 0, 0)$	$(0, 1, 0)$
	3	$(0, 0, -a^*)$	$(0, 0, -1)$
(b) Nd sublattice (modes multiplied by $\sqrt{3}$): $\tau = \tau_1 + \tau_2 + \tau_3$			
Atom no (position)	j	$\mathbf{\Psi}_j(\mathbf{k})$	$\mathbf{\Psi}_j(-\mathbf{k})$
1 $(0, 0, 0)$	1	$(b^*, -i, 0)$	$(-b^*, -b, 0)$

Appendix B

Table B.1. Irreducible representations τ_s and magnetic modes $\mathbf{\Psi}_{jm}$, as obtained from the program MODY [17] for the two-dimensional irreducible representation τ_3 and $\mathbf{k} = [0, 0, 3/2]$, $a = \exp(i\pi/3)$, $b = \exp(i\pi/6)$.

Sym. op./ Irred. rep.	1	3^+	3^-	$2_{[010]}$	$2_{[100]}$	$2_{[110]}$
τ_1	1	1	1	1	1	1
τ_2	1	1	1	-1	-1	-1
τ_3	$\begin{pmatrix} 1 & 0 \\ 0 & 1 \end{pmatrix}$	$\begin{pmatrix} -a^* & 0 \\ 0 & -a \end{pmatrix}$	$\begin{pmatrix} -a & 0 \\ 0 & -a^* \end{pmatrix}$	$\begin{pmatrix} 0 & 1 \\ 1 & 0 \end{pmatrix}$	$\begin{pmatrix} 0 & -a^* \\ -a & 0 \end{pmatrix}$	$\begin{pmatrix} 0 & -a \\ -a^* & 0 \end{pmatrix}$

(a) Fe sublattice (there is only one orbit): representation $\tau = \tau_1 + 2\tau_2 + 3\tau_3$

	$\mathbf{\Psi}_{jm}(\mathbf{k})$ atom 1	$\mathbf{\Psi}_{jm}(\mathbf{k})$ atom 2	$\mathbf{\Psi}_{jm}(\mathbf{k})$ atom 3
jm	$(x, 0, 0)$	$(0, x, 0)$	$(1 - x, 1 - x, 0)$
1a	$(1, 0, 0)$	$(0, -a, 0)$	$(a^*, a^*, 0)$
1b	$(-a^*, 0, 0)$	$(0, -a, 0)$	$(-1, -1, 0)$
2a	$(0, 1, 0)$	$(a, a, 0)$	$(-a^*, 0, 0)$
2b	$(a^*, a^*, 0)$	$(-a, 0, 0)$	$(0, 1, 0)$
3a	$(0, 0, 1)$	$(0, 0, -a)$	$(0, 0, -a^*)$
3b	$(0, 0, a^*)$	$(0, 0, a)$	$(0, 0, -1)$
4a	$(a, a, 0)$	$(-a^*, 0, 0)$	$(0, 1, 0)$
4b	$(0, 1, 0)$	$(a^*, a^*, 0)$	$(-a, 0, 0)$

(b) Nd sublattice (modes multiplied by $2\sqrt{3}$): $\tau = \tau_2 + \tau_3$

	$\mathbf{\Psi}_{jm}(\mathbf{k})$ atom 1
jm	$(0, 0, 0)$
1a	$(b^*, -i, 0)$
1b	$(-b^*, -b, 0)$

References

[1] Campá J A, Cascales C, Gutiérrez-Puebla E, Monge M A, Rasines I and Ruíz-Valero C 1997 *Chem. Mater.* **9** 237
[2] Chukalina E P, Kuritsin D Yu, Popova M N, Bezmaternykh L N, Kharlamova S A and Temerov V L 2004 *Phys. Lett.* A **32** 239
[3] Balaev A D, Bezmaternykh L N, Gudim I A, Temerov V L, Ovchinnikov S G and Kharlamova S A 2003 *J. Magn. Magn. Mater.* **258–259** 532
[4] Pankrats A I, Petrakovskii G A, Bezmatgernykh L N and Bayukov O A 2004 *JETP* **99** 766
[5] Kadomtseva A M, Popov Yu F, Krotov S S, Zvezdin A K, Vorob'ev G P, Bezmaternykh L N and Popova E A 2005 *Fiz. Nizk. Temp. (Ukraine J. Phys. Low Temp.)* **31** 1059
[6] Yen F, Lorenz B, Sun Y Y, Chu C W, Bezmaternykh L N and Vasiliev A N 2006 *Phys. Rev.* B **73** 054435
[7] Klimin S A, Fausti D, Meetsma A, Bezmaternykh L N, van Loosdrecht P H M and Palstra T T M 2006 *Preprint* cond-mat/0502423
[8] Bartl M H, Gatterer K, Cavalli E, Speghini A and Bettinelli M 2001 *Spectrochim. Acta* A **57** 1981
[9] Hur N, Park S, Sharma P A, Ahn J S, Guha S and Cheong S-W 2004 *Nature* **429** 392
[10] Khomskii D I 2006 *J. Magn. Magn. Mater.* at press (Topical Review)
(Khomskii D I 2006 *Preprint* condmat/0601696)
[11] Bezmaternykh L N, Kharlamova S A and Temerov V L 2004 *Krystallografiya* **49** 945
[12] Fischer P, Frey G, Koch M, Könnecke M, Pomjakushin V, Schefer J, Thut R, Schlumpf N, Bürge R, Greuter U, Bondt S and Berruyer E 2000 *Physica* B **276–278** 146
[13] Fischer P, Keller L, Schefer J and Kohlbrecher J 2000 *Neutron News* **11** 19
[14] Schefer J, Könnecke M, Murasik A, Czopnik A, Strässle Th, Keller P and Schlumpf N 2000 *Physica* B **276–278** 168
[15] Rodriguez-Carvajal J 1993 *Physica* B **192** 55
[16] Izyumov Yu A and Naish V E 1979 *J. Magn. Magn. Mater.* **12** 239
[17] Sikora W, Bialas F and Pytlik L 2004 *J. Appl. Crystallogr.* **37** 1015
[18] Dowty E 2006 Program ATOMS, Shape Software
[19] Darby M I 1967 *Br. J. Appl. Phys.* **18** 1415